



## Article

# Experimental Study on Chloride-Induced Corrosion of Soil Nail with Engineered Cementitious Composites (ECC) Grout

Haoliang Wu <sup>1,\*</sup>, Jing Yu <sup>2</sup>, Jiajia Zhou <sup>3</sup>, Weiwen Li <sup>4</sup> and Christopher K. Y. Leung <sup>1</sup>

- <sup>1</sup> Department of Civil and Environmental Engineering, Hong Kong University of Science and Technology, Hong Kong 999077, China; ckleung@ust.hk
- <sup>2</sup> School of Civil Engineering, Sun Yat-sen University, Guangzhou 510275, China; yujing63@mail.sysu.edu.cn
- <sup>3</sup> School of Civil and Environmental Engineering, Zhengzhou University, Zhengzhou 450001, China; zhouaf@zzu.edu.cn
- <sup>4</sup> Guangdong Provincial Key Laboratory of Durability for Marine Civil Engineering, Shenzhen University, Shenzhen 518060, China; liweiwen@szu.edu.cn
- \* Correspondence: wuhaoliang@ust.hk

**Abstract:** Conventionally, a soil nail is a piece of steel reinforcement installed inside a hole drilled into the slope and filled with cement paste (CP) grout. Chloride penetration is a major deterioration mechanism of conventional soil nails as the CP grout is easy to crack with an uncontrollable crack opening when the soil nail is subject to loading or ground movements. Engineered Cementitious Composites (ECC) are a class of fiber-reinforced material exhibiting excellent crack control even when loaded to several percent of strain, and therefore, ECCs have great potential to replace traditional CP grout in soil nails for achieving a long service life. In this study, the chloride ion transport characteristics and electrically accelerated corrosion process of steel rebar in ECC and CP grouts are systematically studied. The rapid chloride ion penetration test results showed a reduction of 76% and 58% passing charges in ECC with 0.15% and 0.3% pre-loading strain, respectively, as compared to that in un-cracked CP. Furthermore, the accelerated corrosion experimental data showed that ECC under pre-loading strain still exhibited a coefficient of chloride ion diffusion that is 20–50% lower than CP grout due to the ability to control crack width. Service life calculations based on experimentally measured parameters showed that the predicted corrosion rate and corrosion depth of soil nails in ECC grout were much lower than those in CP grout. The findings can facilitate the design of soil nails with excellent durability and long service life.

**Keywords:** engineered cementitious composite (ECC); soil nail; chloride-induced corrosion; durability; chloride diffusion coefficient



**Citation:** Wu, H.; Yu, J.; Zhou, J.; Li, W.; Leung, C.K.Y. Experimental Study on Chloride-Induced Corrosion of Soil Nail with Engineered Cementitious Composites (ECC) Grout. *Infrastructures* **2021**, *6*, 161. <https://doi.org/10.3390/infrastructures6110161>

Academic Editors: Suvash Chandra Paul and Gideon van Zijl

Received: 22 September 2021  
Accepted: 3 November 2021  
Published: 10 November 2021

**Publisher's Note:** MDPI stays neutral with regard to jurisdictional claims in published maps and institutional affiliations.



**Copyright:** © 2021 by the authors. Licensee MDPI, Basel, Switzerland. This article is an open access article distributed under the terms and conditions of the Creative Commons Attribution (CC BY) license (<https://creativecommons.org/licenses/by/4.0/>).

## 1. Introduction

Rainfall-triggered landslides in mountainous regions around the world have produced a large number of casualties and serious damages [1–4]. It is, therefore, necessary to provide a rational and reliable strategy to improve slope stability. One possible and economical way to stabilize geotechnical structures, such as soil slopes, excavations and retaining walls, is through the use of a soil-nailing technique [5,6]. The soil nails are placed in the active zone to offer sliding resistance along the identified potential failure surface. Soil nails usually consist of steel reinforcing bars placed in a drilled hole filled with cement paste (CP) grout. The steel bar is installed at an inclination of 10 to 20 degrees with the horizontal to resist tension, shear and bending loads. The various merits of soil nails compared to concrete retaining walls, such as quicker construction, lower cost and less environmentally destructive, have led to its widespread use in Hong Kong [7,8].

In a conventional soil nail system, the steel bar is protected against direct exposure to soil masses by the CP grout. Water and chemicals, however, can pass through the grout and reach the steel bar surface. The situation is particularly harmful if there is

a high concentration of chloride ions in the soil mass. Chloride ingress into CP grout involves several transport processes, such as capillary suction, diffusion, permeation and migration [9]. Due to the brittleness of CP grout, it is easy for cracks to form under loading or ground movement. With poor control of crack opening, the rate of chloride penetration is greatly increased. Once the chloride ion concentration reaches a threshold level high enough to disrupt the passive film on the rebar surface, corrosion begins to occur [10]. In Hong Kong, the corrosion of soil nails has been reported in a number of case studies [11]. Apart from providing sacrificial steel thickness, corrugated plastic sheaths are utilized in combination with cement grout when a high level of corrosion protection is required [11]. The installation of the sheath inhibits the entrance of water or caustic chemicals if the grout cracks. The addition of a corrugated plastic sheath, on the other hand, considerably raises the cost and difficulty of construction. To improve the service life and reduce the cost of soil nails, a new design of the soil nailing system is to replace the brittle cement grout with Engineered Cementitious Composites (ECC).

ECC is a class of fiber-reinforced material exhibiting excellent crack control even when loaded to several percent of strain [12–15]. The crack width, typically below 60 microns, does not raise the water permeability or chloride diffusivity significantly beyond that of the uncracked material [16]. In addition, these fine cracks can be self-healed under flowing water [17,18]. By replacing conventional CP grout with ECC to control crack width, the service life is expected to be significantly improved. Researchers [19] found that the addition of 55–70% fly ash in ECC significantly decreased chloride diffusion coefficient ( $D$ ). The use of fly ash probably resulted in a denser matrix by reducing the pore size and thickness of the transition zone between fiber or sand and the surrounding cementitious matrix [20]. In the existing literature, most experiments of chloride diffusion in ECC were carried out under normal soaking or dry-wet cycles on dumbbell-shaped laboratory-size specimens [21]. However, the complex chloride diffusion behavior and corrosion process for the larger soil nail is not yet fully understood.

This paper aims to determine the chloride-induced corrosion process of the embedded steel rebar in the soil nailing system. The comparison of grout materials (CP vs. ECC) and different pre-loading conditions are investigated. Knowing the chloride diffusivity, the corrosion depth of steel rebars in CP and ECC grouts exposed to salt-laden environments for 120 years is predicted. The results would yield useful information on the durability of soil nails in geotechnical applications.

## 2. Materials and Test Methods

### 2.1. Mix Composition

Table 1 lists the blending proportions of conventional CP grout and ECC (by weight of binder). The matrix components included CEM I Portland cement (Grade 52.5N, BS EN 197-1 [22]), fly ash, tap water, and polycarboxylate-ether superplasticizers (SP). Table 2 provides the chemical compositions of cement and fly ash. The polyvinyl alcohol fibers produced by Kuraray Co., Ltd. (Tokyo, Japan) were used to reinforce the matrix in the ECC. A mass ratio of 0.8% GCP™ ADVA 189 SP was utilized to tailor the fresh property of the mixtures. The polyvinyl alcohol fiber is around 39  $\mu\text{m}$  and 8 mm in diameter and length, respectively. The ultimate tensile strength is 1600 MPa, and Young's modulus is 42.8 GPa. SP provided by Grace™ was used to control the workability of the ECC mixes and ensure the good dispersion of fibers. The SP content (0.8%), FA/PC ratio (2.0) and fiber content (1.25%) were all fixed in this investigation based on the CP's equivalent flowability with a min-slump flow test [13]. A truncated cone with a dimension of 60 mm height, 100 mm bottom diameter and 70 mm top diameter was filled with fresh mixtures and lifted upward immediately. The min-slump flow test was repeated twice to get an average value. The average diameters of the fresh CP and ECC mixtures were 23.87 and 23.14 cm, respectively.

**Table 1.** Mix proportion of the specimens (mass ratio).

	Cement	Fly Ash	Water/Binder	SP (%)	Fiber <sup>a</sup> (vol.%)	Ave. Diameter <sup>b</sup> (cm)
Cement Paste	1	0	0.4	0	0	23.87
ECC	1	2	0.9	0.8	1.25%	23.14

<sup>a</sup> Polyvinyl alcohol fiber proportion by volume. <sup>b</sup> Average diameter is obtained by min-slump flow test.

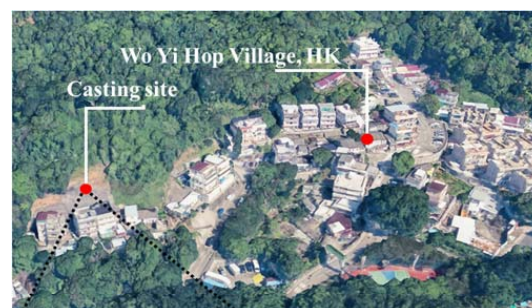
**Table 2.** Chemical Composition of Portland cement and fly ash (by mass).

Materials	Al <sub>2</sub> O <sub>3</sub> (%)	SiO <sub>2</sub> (%)	CaO (%)	Fe <sub>2</sub> O <sub>3</sub> (%)	SO <sub>3</sub> (%)	MgO (%)	Na <sub>2</sub> O (%)	K <sub>2</sub> O (%)	LOI <sup>a</sup> (%)
Cement	4.4	20.2	63.9	3.4	4.7	2.1	0.1	0.4	1.2
Fly ash	16.0	52.1	14.1	6.4	0.59	4.8	1.72	2.4	0.1

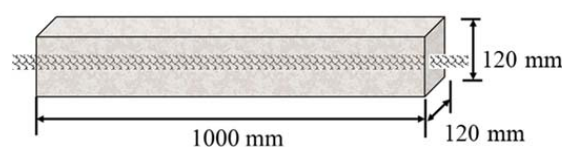
<sup>a</sup> LOI: Loss on Ignition.

**2.2. Specimens Preparation and Test Methods**

Rectangular panel specimens were prepared in the field (Figure 1a) using site equipment for pumping and grouting. The dimension of specimens was 1000 mm length, 120 mm width and 120 mm height, as shown in Figure 1b. The diameter of the rebar was 16 mm. The fresh CP and ECC grouts were first mixed by a concrete mixer at 150 rpm, and then pumped into rectangular molds (in the form of a box) through a hose and nozzle. The pump rate was set at approximately ~1.5 cubic meters per hour. The grout pipe was placed in the middle of the rectangular mold. After hardening, testing specimens were obtained from the two sides of the pipe. The CP and ECC grouts were cured at the casting site for 28 days and then moved to the laboratory for the chloride ion penetration and chloride ion corrosion tests.



(a)



(b)

**Figure 1.** The onsite casting of CP and ECC grouts (a) and the dimension of samples (b).

### 2.2.1. Rapid Chloride Ion Penetration Test

After 28 days of curing, the rapid chloride ion penetration test (RCPT), according to ASTM C1202-12 [23], was adopted for all mixes in this study. Disk-shape cement paste grout and ECC samples with a dimension of 100 mm in diameter were obtained by coring from the grouted panel. All disk-shaped samples were further polished by a water-cooled diamond saw until the height of the specimen became 50 mm. To study the effect of cracking on chloride ion penetration, the disk-shaped samples were fractured by splitting tension under vertical loading in an MTS machine (Figure 2). The loading rate was kept constant at 0.02 mm/s. The horizontal displacement was continuously monitored using two LVDTs, which were positioned at opposite sides of the specimen (Figure 2). Various samples were pre-loaded to tensile strains of 0%, 0.15%, and 0.3% along the centerline of the specimens. The pre-loaded samples were denoted as PC-0%, ECC-0%, ECC-0.15% and ECC-0.3%, respectively. Four replicates were prepared for each pre-loaded group.



Figure 2. Splitting tension setup used to fracture ECC disk-shaped specimens.

After fracturing, the specimens were placed in a vacuum saturation apparatus for 3 h and then immersed in water for 18 h under natural ambient pressure. Then, the cylindrical surface of the specimens was covered with epoxy coating before each specimen was sandwiched into the RCPT set up, as shown in Figure 3. One side of the cells was filled with 3.0% (wt.%) NaCl solution and the other with 1.2% (wt.%) NaOH solution. A DC voltage of 60 V was applied between the specimen’s two sides to determine the electrical conductance in coulombs. The passed charge was recorded per 30 min over a 6-h period to provide a rapid indication of chloride ion penetrability.

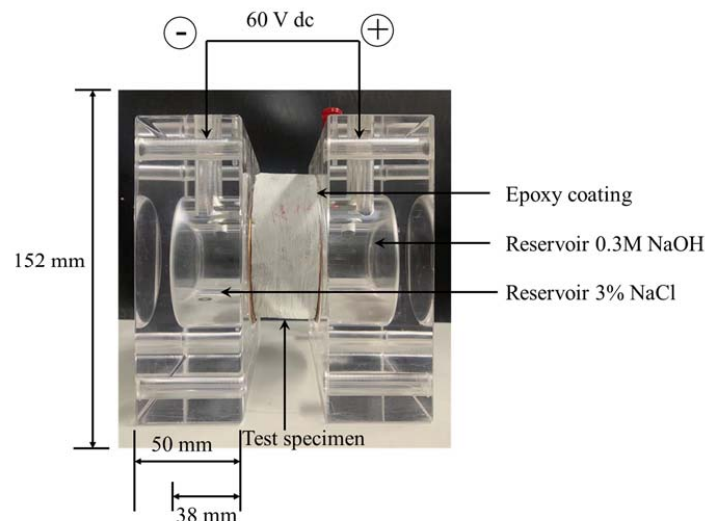


Figure 3. Rapid chloride ion penetration test cell.

After the rapid chloride penetrability test, the specimens were split to measure the penetration of chlorides by using the colorimetric method. A silver nitrate aqueous solution (0.1 mol/L AgNO<sub>3</sub>) was sprayed on one split surface of the specimens to reveal the depth of chloride penetration ( $X_d$ ). The chloride diffusion coefficient ( $D$ ) under non-steady-state migration was calculated from  $X_d$  according to the Bassuoni et al. [24] and Edvardsen et al. [25] via Equation (1):

$$D = \frac{0.0239(273 + T)L}{(V - 2)t} \left( X_d - 0.0238 \sqrt{\frac{(273 + T)LX_d}{V - 2}} \right) \quad (1)$$

where  $D$  is the non-steady-state diffusion coefficient ( $\times 10^{-12} \text{ m}^2/\text{s}$ ),  $V$  is applied voltage (V),  $T$  is the average value of initial and final temperatures in the solution ( $^{\circ}\text{C}$ ),  $L$  is the thickness of the specimen (mm),  $X_d$  is the average value of penetration depth (mm) and  $t$  is the time (h).

### 2.2.2. Impressed Voltage Accelerated Corrosion Test

To study the ECC grout soil nails under various cracking conditions, rectangular specimens with the rebar in the middle were pre-loaded under uniaxial tension with prescribed tensile strains of 0%, 0.15% and 0.30%. Three replicates were prepared for each prescribed group. During the testing, a controlled displacement rate of 0.2 mm/min was adopted, and two linear variable displacement transducers (LVDTs) were attached on opposite sides of each specimen to quantify the tensile deformation, as shown in Figure 4. After the loaded specimen was removed from the testing machine, it was placed in contact with 5% NaCl solution in a container and an external direct current source with 20 V constant voltage was applied to the rebar to accelerate the steel corrosion process. In this test, the steel rebar contacted the anode, and the NaCl solution served as the cathode. During the accelerated corrosion process, the impressed current was measured and recorded every 2 h. This test would be ended when the impressed current reaches a steady condition.

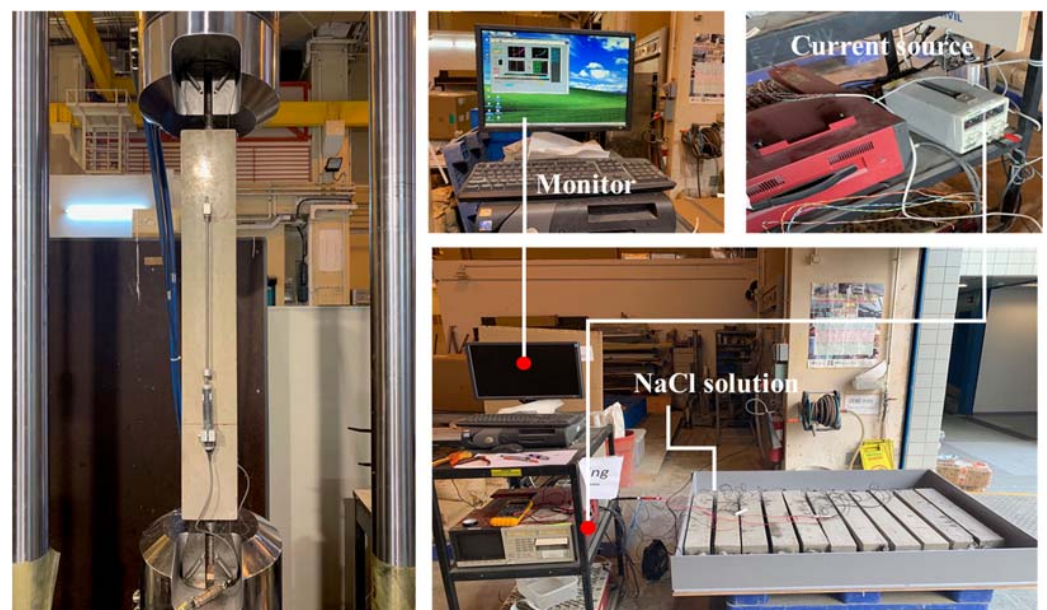


Figure 4. Pre-loading and accelerated corrosion test setup for cement paste and ECC specimens.

### 3. Results and Discussion

#### 3.1. Passing Charges

The results of the rapid chloride ion penetrability test on day 28 are given in Figure 5. It could be seen that the passing charge increased with increasing prescribed strains of the specimens due to the larger cracks. The total passing charges through the ECC specimens were 2850, 4180 and 7540 coulombs under prescribed strains of 0%, 0.15% and 0.3%, respectively. Namely, the passing charge increased 1.47–2.65 times as the prescribed strains increased from 0% to 0.3%. It was noticed that the ECC-0% performed better than virgin CP grout in the resistance to chloride ion penetration. This is attributed to the lower average pores in ECC, which inhibit the transportation of chloride [26]. Moreover, the incorporation of fly ash in ECC may enhance the resistance of chloride penetration in cementitious materials, as the pozzolanic reaction results in fewer capillary pores and reduces the transport of chloride ions [27]. In comparison to CP-0%, the increase of the passing charges in ECC-0.15% and ECC-0.3% are 24% and 42%, respectively. The qualitative indications of the chloride ion penetrability based on the measured values from this test method are provided in Table 3. The results indicated that the chloride permeability level for virgin CP, ECC-0% and ECC-0.15% grouts were high, but that for the ECC-0% was a moderate level.

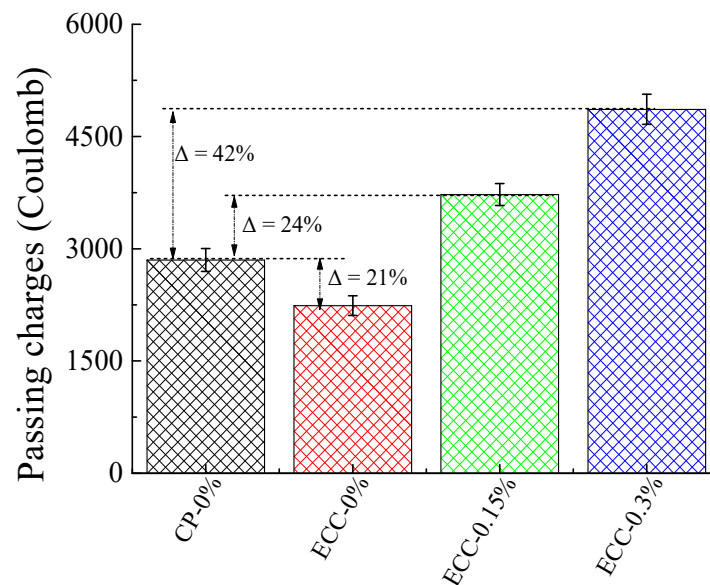


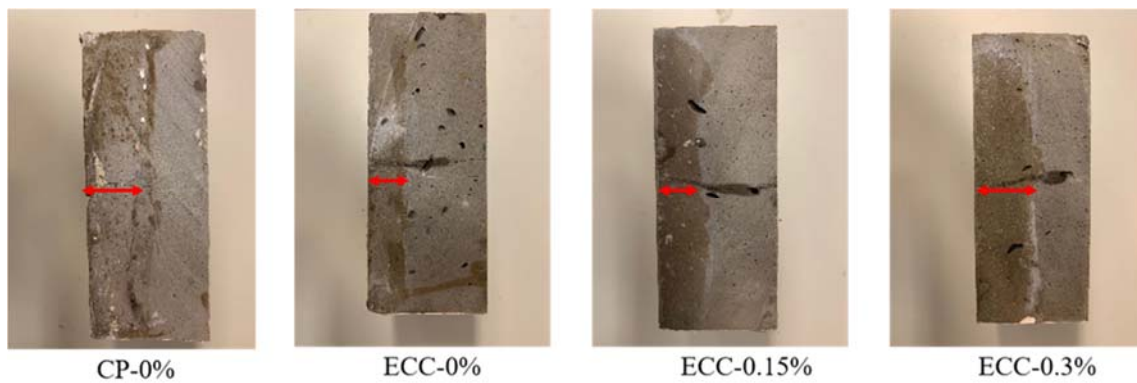
Figure 5. Total charges passed through CP and ECC grouts at 28-days curing. ECC specimens were significantly lower than CP specimens for the total passed charges.

Table 3. Chloride permeability based on charge passed (as per ASTM C1202 [23]).

Charge Passed (Coulombs)	Chloride Permeability Level
>4000	High
2000–4000	Moderate
1000–2000	Low
100–1000	Very low
<100	Negligible

#### 3.2. Chloride Diffusion Coefficient

The chloride penetration depth was measured from the visible white silver chloride precipitation, as shown in Figure 6. The average depths of chloride migrating into CP-0% was 33 mm, while the values for ECC were 17, 20 and 25 mm under prescribed strains of 0%, 0.15% and 0.3%, respectively.



**Figure 6.** Chloride front migrating into CP and ECC specimens.

The diffusion coefficient results obtained from the aforementioned Equation (2) are summarized in Figure 7. The diffusion coefficient was  $1.86 \times 10^{-11} \text{ m}^2/\text{s}$  in CP-0% grout. For the ECC specimens, while a higher diffusion coefficient is induced by increased prescribed strains, the measured values up to 0.3% were all lower than that for CP-0% grout. The diffusion coefficients of ECC under prescribed strains of 0%, 0.15% and 0.3% were 50%, 41% and 25% lower than those of CP grout, respectively. Previous research showed that the incorporation of fly ash in cement materials could reduce the diffusivity of chloride ions due to the densification of the pore size structure in the hydration products [28]. In addition, the fly ash in ECC formed more  $\text{C}_3\text{A}$  than CP grout, which could facilitate the adsorption of more chloride ions to form the Friedel’s salt ( $\text{C}_3\text{A}\cdot\text{CaCl}_2\cdot 10\text{H}_2\text{O}$ ) [29]. From the results of the current study, it is apparent that the ECC grout is more robust than conventional CP grout against chloride ion penetration.

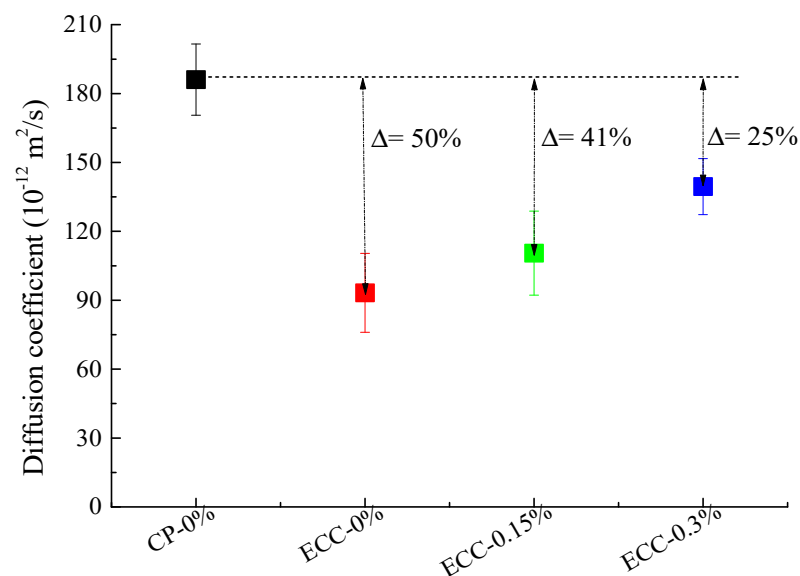


**Figure 7.** Diffusion coefficients of CP and ECC grouts under various prescribed strains.

### 3.3. Impressed Current and Ohmic Resistance

Figure 8 illustrates the impressed current versus exposure time for the steel bar in ECC and CP grouts under the fixed potential. Each line in Figure 8 represents the average of three specimens. A two-stage procedure of current-time can be observed. The impressed current of all specimens first increased with the testing time (Phase I) and then reached a steady stage (Phase II). Because the specimens were soaked in tap water and saturated before the accelerated corrosion test, the same value of the initial current was recorded for the ECC and CP specimens. During the corrosion progress, the negatively charged chloride ions from the solution were attracted toward the positively charged steel bar as

the electrical potential was applied to the soil nails. Eventually, the steel bar surface began to corrode as the chloride ions reached a critical concentration at the soil nail surface. As the increased corrosion products diffused along the cracks and gradually filled the pores of CP grout or ECC surrounding the rebar, the impressed current increased (Phase I). As seen from Figure 8, the current recorded for all ECC and CP specimens achieved approximately 170–180 mA at 180 h. After 100 h, a lower current was recorded in the cracked ECC (ECC-0.15% and ECC-0.3%) compared with the undamaged ECC. However, at around 180 h, all specimens reached the steady-state in Phase II, and the recorded current was about the same (Figure 8). This might be attributed to the continuous oxygen reaction occurring at a steady speed. In this study, the presence of a steady-state (Phase II) reflected that the corrosion rate had reached the maximum value.

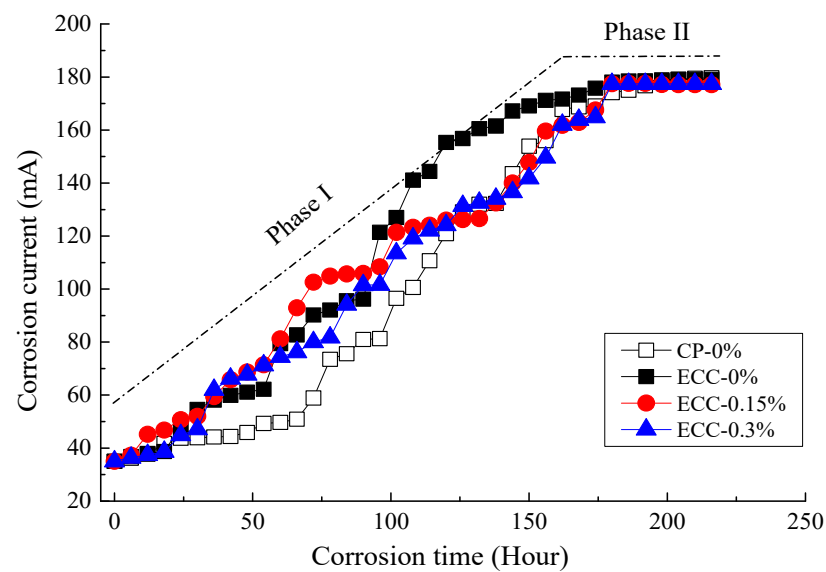


Figure 8. Impressed current versus exposure time for the CP and ECC grouts.

During the early stage of corrosion, the oxides that formed the passive film on the steel rebar were thermodynamically stable in the alkaline environment around the soil nail. As the chloride ions built up around the steel rebar, the corrosion tended to be localized, and the chloride-induced corrosion initiation followed the model of pitting corrosion. However, it is generally known that pit nucleation is typically accompanied by passivation. The chloride ions bound in the steel rebar may induce corrosion, whereas the hydroxyl ions bound in the solid phase prevent corrosion [30,31]. In the corrosion progress, the anodic reaction was the oxidation process that leads to a dissolution or loss of metal, while the cathode reaction was the process of reduction that leads to the formation of a hydroxyl ion from dissolved oxygen. For steel rebar embedded in CP and ECC grouts, the anodic reactions depended on the pH of the interstitial electrolyte, the presence of aggressive anions and the existence of an appropriate electrochemical potential at the steel surface [32,33]. As illustrated in Figure 9, evident corrosion products are detected on the surface of metallic rebar regardless of CP or ECC.



Figure 9. Corrosion phenomenon of CP and ECC specimens after the impressed current test.

The ohmic resistance ( $R_s$ ) for all specimens during the corrosion progress can be calculated from Equation (2).

$$R_s = \frac{U}{I} - R_0 \tag{2}$$

where  $R_s$  is the ohmic resistance of CP and ECC grouts during the corrosion progress (ohm),  $U$  is the constant DC voltage (20 V) and  $I$  is the recorded current in Figure 8.  $R_0$  is the ohmic resistance of an extra resistor for each specimen to avoid a large current in the circuit, and the value is shown in Table 4.

**Table 4.** Ohmic resistance of the extra resistor ( $R_0$ ).

Samples	CP-0%	CP-0.15%	CP-0.3%	ECC-0%	ECC-0.15%	ECC-0.3%
Resistivity $\Omega/m$	111.2	112.0	112.5	111.5	112.5	112.1

Figure 10 shows the calculated  $R_s$  development for the CP and ECC grouts during various corrosion periods. It could be seen that the  $R_s$  gradually decreased with increasing exposure time. As pre-loaded strain increased from 0% to 0.15% and 0.3%, the  $R_s$  for ECC specimens were quite close to each other irrespective of their pre-loading strain. Whereas the  $R_s$  for CP-0% was higher than both the uncracked and cracked ECC over most of the corrosion period.

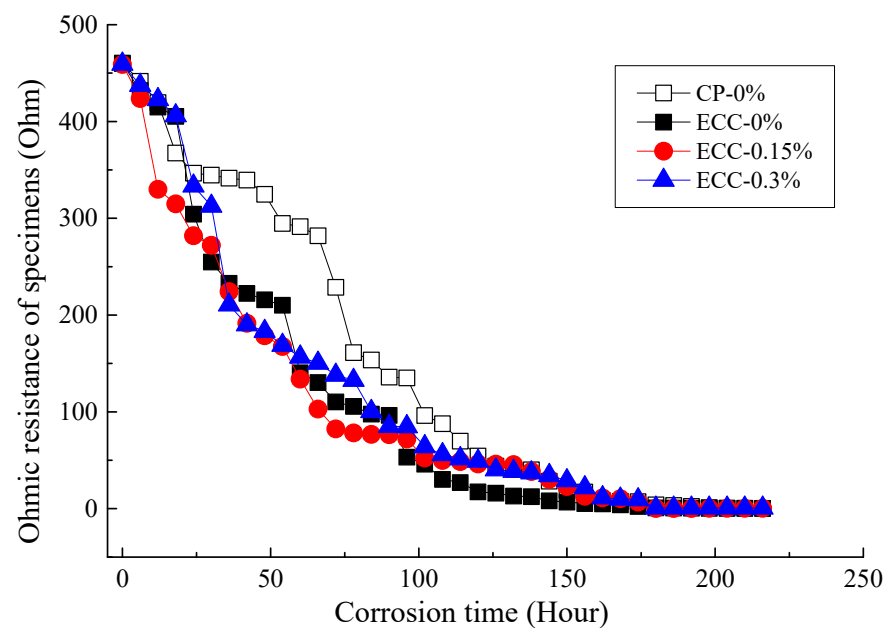


**Figure 10.** Ohmic resistance of specimens versus exposure time for the CP and ECC grouts.

### 3.4. Prediction of Chloride Concentration on Steel Surface and Corrosion Rate

To analyze the effects of grout materials and pre-loading strain on the service life of soil nails as exposed to the extreme chloride condition, the schematic of a soil nail under the chloride exposure is illustrated in Figure 11. The diameter of the rebar and grout cylinder is 16 and 89 mm, respectively. The chloride ion penetration occurs either through the capillary pores or cracks by permeation, capillary suction and diffusion. This transport process has been extensively explored, and several models have been developed to predict the chloride penetration profiles [10,28,32]. Most of these models are based upon Fick’s second law and has been widely applied in the engineering and research aspect. In this study, three assumptions are made to simplify the problem: (i) diffusion is taken to be the major process, (ii) the cracks are not explicitly considered, but their presence will lead to an effective increase in diffusion coefficient as measured in the tests described in Section 3.2 and

(iii) axisymmetric diffusion in the real situation is simplified into unidirectional diffusion (from outer grout surface into rebar surface) in a semi-infinite domain.

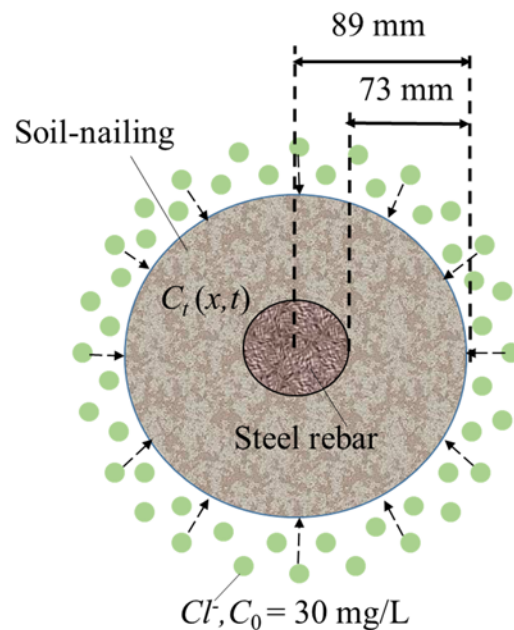


Figure 11. Schematic of a soil nail under chloride attack.

The diffusion of chloride ions into concrete can then be described by Crank’s solution to Fick’s second law [34–37]. This law for a one-dimensional case is:

$$\frac{\partial C}{\partial t} = D \frac{\partial^2 C}{\partial x^2} \tag{3}$$

where  $C$  is the concentration,  $D$  is the diffusion coefficient,  $t$  is the diffusion duration and  $x$  is the diffusion distance. For unidirectional flow, the solution of this equation is as follows:

$$C(x, t) = C_0 \left( 1 - \operatorname{erf} \frac{x}{2\sqrt{Dt}} \right) \tag{4}$$

where  $C(x, t)$  is the chloride concentration at a distance  $x$  (mm) from the outside surface at corrosion time  $t$  (s),  $C_0$  is the chloride concentration (30 mg/L) on the outside surface of the grout and  $\operatorname{erf}$  is the error function.

Equation (3) assumed that the grout is homogenous, and the diffusion coefficient  $D$  is independent of chloride concentration and temperature ( $T$ ). In fact, for a certain interval period, this second law of Fick’s has been found to be a fair estimate for the depth of chloride in a homogenous structure either exposed to the ambient state of the atmosphere and/or submerged. The solution given by Equation (4) is valid only if the boundary and material properties are constant. The initial condition is  $C_l(x, t) = 0$  when  $x > 0$  and  $t = 0$ , and  $C_l(x, t) = C_0$  for  $x = 0$  and  $t = 0$ . In this study, we assumed that the chlorides in the grout are not present initially, and the chlorides in the system are totally from the exposure condition.

In this case, the service life of soil nails would be designed as 120 years. As shown in Figure 11, the chloride transportation distance to the rebar surface is 73 mm,  $C_0$  is assumed to be 30 mg/L and the diffusion coefficient  $D$  of CP and ECC grouts are obtained from Figure 7. Based on calculations from Equation (4), the predicted results of chloride concentration on the rebar surface are shown in Figure 12. Specifically, the chloride concentration on the rebar surface for CP and ECC grouts with different pre-loading conditions after 120-years of exposure was illustrated. The results in Figure 12 demonstrated that larger pre-loading conditions in grout resulted in higher chloride concentration on the surface of

the steel rebar. With good crack control, as well as lower diffusivity in the uncracked state, the ECC grouts loaded to 0.15% and 0.30% strain still exhibit chloride concentration on the steel rebar surface than the virgin CP grout.

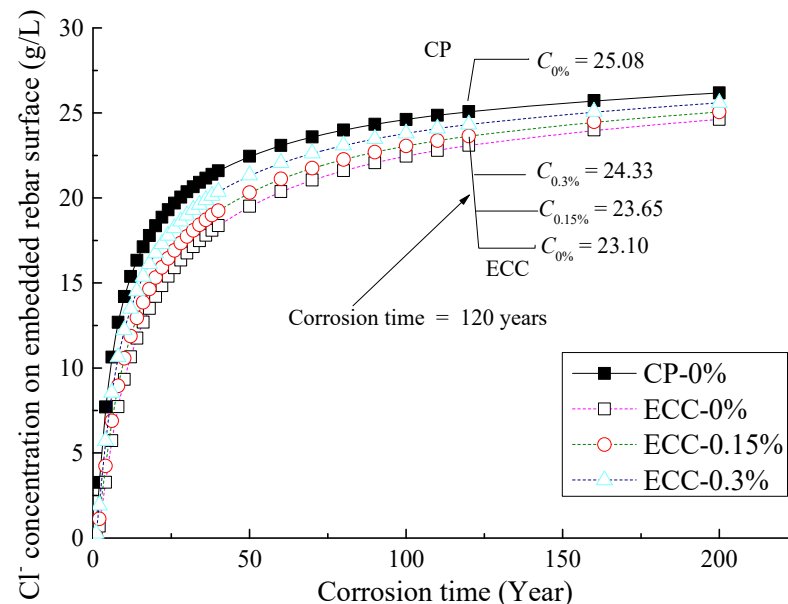


Figure 12. Predicted chloride concentration on the surface of rebars based on Fick’s second law.

Corrosion penetration in the steel rebar is calculated next. The rates of corrosion varied with changes in the temperature, the quantity of chloride in the surrounding grounds, the resistance to chloride of the grout materials and the duration for corrosion. Based on Liu and Weyers’s [35] statistical analysis, the experimental corrosion rate is shown in Equation (5) with consideration of the concrete temperature, ohmic resistance, chloride content on the surface of steel bar and exposure time:

$$\ln 1.08i = 8.37 + 0.618 \ln 1.69C_{cl} - \frac{3034}{T} - 0.000116R + 2.23t^{-0.215} \quad (5)$$

where  $i$  is the steel corrosion current ( $\mu\text{A}/\text{cm}^2$ ),  $C_{cl}$  is chloride content on the surface of steel at a given time ( $\text{kg}/\text{m}^3$ ),  $T$  is the temperature at the steel surface (Kelvin),  $R$  is the ohmic resistance of the cover concrete (ohms) and  $t$  is corrosion time (years).

It should be noted that the values of chloride content  $C_{cl}$  on the surface of steel at different times were obtained from Figure 12, which represent an extreme condition for soil nails exposed to a natural condition in Hong Kong (with  $C_0 = 30 \text{ mg}/\text{L}$ ).  $T$  is kept at 296.45 Kelvin for the average temperature in Hong Kong. The ohmic resistance of CP and ECC (cracked and loaded to 0.15% and 0.30%) were obtained from the steady value in Figure 10.

The corrosion rate of the steel rebar in soil nails is calculated from the predicted empirical Equation (6) [38] and shown in Figure 13. It can be found from the figure that the corrosion rate in ECC specimens is lower than that in CP. To find the corrosion depth ( $H$ ) of the steel rebar, the corrosion rate in  $\mu\text{A}/\text{cm}^2$  can be transformed into the corrosion rate in  $\mu\text{m}/\text{year}$  through Equation (6). Then, the corrosion depth ( $H$ ) in the predicted 120 years can be calculated by Equation (7).

$$1 \mu\text{A}/\text{cm}^2 = 10 \text{ mA}/\text{m}^2 = 11.6 \mu\text{m}/\text{year} \quad (6)$$

$$H = \sum_{i=1}^{120} I_t \times (t_i - t_{i-1}) \quad (7)$$

where the  $H$  is the corrosion depth ( $\mu\text{m}$ ) and  $I_t$  is the corrosion current ( $\mu\text{A}/\text{cm}^2$ ) at various corrosion times  $t$  (year).

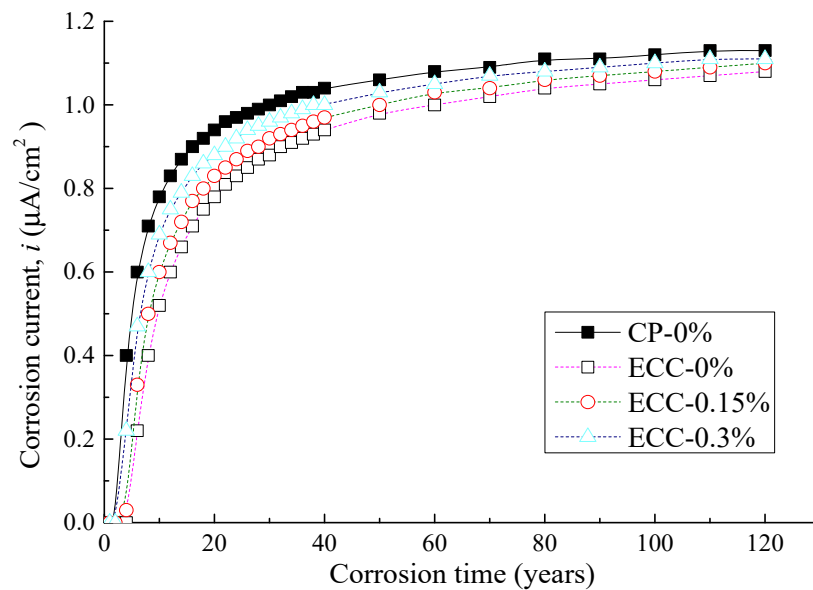


Figure 13. Corrosion rates of steel rebar in soil nails calculated from the empirical equation.

The results of the predicted corrosion depth of rebars in CP and ECC grouts are presented in Figure 14. It could be seen that the corrosion depth of CP-0% grout specimen was 3.05 mm. For the ECC specimens, the 120-year corrosion depth was 2.75, 2.84 and 2.94 mm under prescribed strains of 0%, 0.15% and 0.3%, respectively. The 120-year corrosion depths of ECC-0%, ECC-0.15% and ECC-0.3% were 9.8%, 6.9% and 3.6% lower than the values of CP-0%, respectively. It should be noted that the corrosion rate used to predict chloride concentration on the surface of rebar was obtained from the maximum value (phase II in Figure 8); therefore, the corrosion rates reported in Figure 14 is probably higher than those in real practice. However, for the purpose of comparison amongst different mixes and because all steel rebars went through the same preparation procedure, we could conclude that the rebar in ECC grout (even loaded to 0.30% strain) has lower corrosion depth than that in un-cracked CP grout under the same environmental conditions.

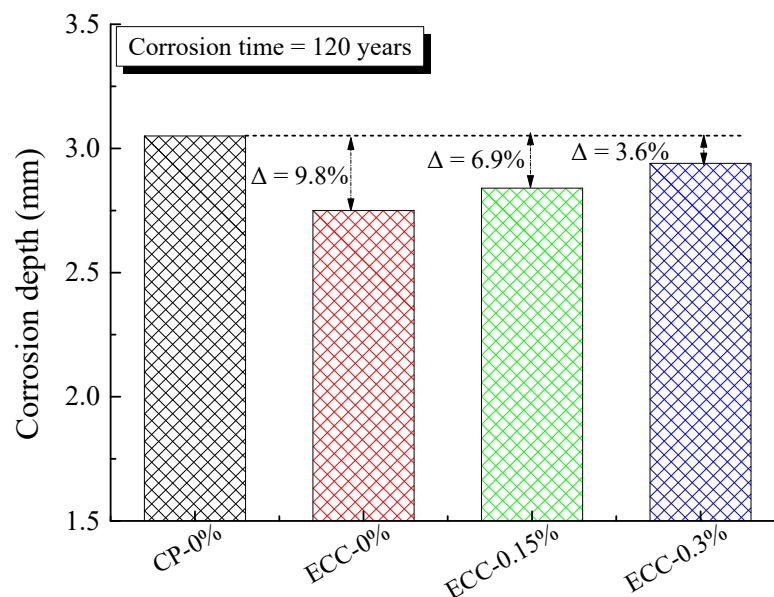


Figure 14. Predicted corrosion depth of soil nails exposed to chloride solution for 120 years.

#### 4. Conclusions

This paper reports the results of a systematic bench-scale study on the chloride ion transport characteristics and chloride-induced corrosion process of steel rebar embedded in ECC and CP soil nails. From this experimental study and simulation results, the following conclusions can be drawn:

1. The rapid chloride ion penetration test showed that the passing charge increased 1.47–2.65 times, and as prescribed, strains increased from 0% to 0.3%. An increment of the passing charges in ECC-0.15% and ECC-0.3% are 24% and 42% as compared to those of CP-0%. The diffusion coefficients of ECC were lower by 25–50% than those of CP grout. It was possible that the tight crack width and denser pore structure retard the transportation of chloride.
2. Impressed voltage accelerated corrosion test showed that a two-stage procedure could be observed during the corrosion period. The impressed current of CP and ECC grouts increased with increasing corrosion time first and then became stable. The ohmic resistance is similar for all cases at the steady-state.
3. Corrosion with an assumed high chloride concentration of 30 mg/L on the outside surface of grouts was simulated for 120 years, the calculation showed that the corrosion depths of ECC grout were 3.6–9.8% lower than that of un-cracked CP when the ECC strain increased from 0% to 0.30%. A novel aspect of this research is to apply the ECC as grout for soil nails. Based on the finding that the corrosion penetration depth of rebar in cracked ECC is lower than that in un-cracked CP grout, there is the potential to remove the plastic sheath around the rebar even under corrosive environments. The construction cost and time can then be significantly reduced. In this study, the mathematical prediction method uses Crank's solution to Fick's second law. Whereas the chloride diffusion conduct occurs in a solid cylinder rather than a semi-infinite domain in the accelerated corrosion test. An advanced diffusion model is warranted to calculate the chloride diffusion through the cylindrical coordinate system in further study.

**Author Contributions:** H.W.: Conceptualization, Investigation, Data Curation, and Writing—Original Draft. J.Y.: Investigation and Writing—Original Draft. J.Z.: Investigation. W.L.: Writing—review and editing. C.K.Y.L.: Supervision and Resources. All authors have read and agreed to the published version of the manuscript.

**Funding:** The research was supported by FRC LLC Ltd. from the US. The sponsor has no role in the design, execution, interpretation, or writing of the paper.

**Institutional Review Board Statement:** Not applicable.

**Informed Consent Statement:** Not applicable.

**Data Availability Statement:** Not applicable.

**Acknowledgments:** The authors express their thanks to the sponsorship by the FRC LLC Ltd. from the US, and Geotechnical Engineering Office in Hong Kong.

**Conflicts of Interest:** The authors declare that they have no known competing financial interest or personal relationships that could have appeared to influence the work reported in this paper.

#### References

1. Kong, V.W.W.; Kwan, J.S.H.; Pun, W.K. Hong Kong's landslip warning system—40 years of progress. *Landslides* **2020**, *17*, 1453–1463. [[CrossRef](#)]
2. Gao, L.; Zhang, L.M.; Cheung, R.W.M. Relationships between natural terrain landslide magnitudes and triggering rainfall based on a large landslide inventory in Hong Kong. *Landslides* **2018**, *15*, 727–740. [[CrossRef](#)]
3. Peng, D.; Xu, Q.; Liu, F.; He, Y.; Zhang, S.; Qi, X.; Zhao, K.; Zhang, X. Distribution and failure modes of the landslides in Heitai terrace, China. *Eng. Geol.* **2018**, *236*, 97–110. [[CrossRef](#)]
4. Peng, D.; Xu, Q.; Zhang, X.; Xing, H.; Zhang, S.; Kang, K.; Qi, X.; Ju, Y.; Zhao, K. Hydrological response of loess slopes with reference to widespread landslide events in the Heifangtai terrace, NW China. *J. Asian Earth Sci.* **2019**, *171*, 259–276. [[CrossRef](#)]

5. Liu, J.; Shang, K.; Wu, X. Stability Analysis and Performance of Soil-Nailing Retaining System of Excavation during Construction Period. *J. Perform. Constr. Facil.* **2016**, *30*, 4014002. [[CrossRef](#)]
6. Wei, W.; Cheng, Y. Soil nailed slope by strength reduction and limit equilibrium methods. *Comput. Geotech.* **2010**, *37*, 602–618. [[CrossRef](#)]
7. Chu, L.-M.; Yin, J.-H. Comparison of Interface Shear Strength of Soil Nails Measured by Both Direct Shear Box Tests and Pullout Tests. *J. Geotech. Geoenviron. Eng.* **2005**, *131*, 1097–1107. [[CrossRef](#)]
8. Zhu, H.-H.; Yin, J.-H.; Yeung, A.T.; Jin, W. Field Pullout Testing and Performance Evaluation of GFRP Soil Nails. *J. Geotech. Geoenviron. Eng.* **2011**, *137*, 633–642. [[CrossRef](#)]
9. Kobayashi, K.; Kojima, Y. Effect of fine crack width and water cement ratio of SHCC on chloride ingress and rebar corrosion. *Cem. Concr. Compos.* **2017**, *80*, 235–244. [[CrossRef](#)]
10. Yu, H.; Hartt, W.H. Effects of Reinforcement and Coarse Aggregates on Chloride Ingress into Concrete and Time-to-Corrosion: Part 1—Spatial Chloride Distribution and Implications. *Corrosion* **2007**, *63*, 843–849. [[CrossRef](#)]
11. Shiu, H.Y.K.; Cheung, R.W.M. Long-term Durability of Steel Soil Nails in Hong Kong. *HKIE Trans.* **2008**, *15*, 24–32. [[CrossRef](#)]
12. Li, V.C. Introduction to Engineered Cementitious Composites (ECC). In *Engineered Cementitious Composites (ECC)*; Springer: Berlin/Heidelberg, Germany, 2019; pp. 1–10.
13. Wu, H.; Yu, J.; Du, Y.; Li, V.C. Mechanical performance of MgO-doped Engineered Cementitious Composites (ECC). *Cem. Concr. Compos.* **2020**, *115*, 103857. [[CrossRef](#)]
14. Yu, J.; Wu, H.-L.; Leung, C.K. Feasibility of using ultrahigh-volume limestone-calcined clay blend to develop sustainable medium-strength Engineered Cementitious Composites (ECC). *J. Clean. Prod.* **2020**, *262*, 121343. [[CrossRef](#)]
15. Zhang, S.; Li, V.C.; Ye, G. Micromechanics-guided development of a slag/fly ash-based strain-hardening geopolymer composite. *Cem. Concr. Compos.* **2020**, *109*, 103510. [[CrossRef](#)]
16. Lepech, M.D.; Li, V.C. Application of ECC for bridge deck link slabs. *Mater. Struct.* **2009**, *42*, 1185–1195. [[CrossRef](#)]
17. Wu, H.-L.; Du, Y.-J.; Yu, J.; Yang, Y.-L.; Li, V.C. Hydraulic conductivity and self-healing performance of Engineered Cementitious Composites exposed to Acid Mine Drainage. *Sci. Total Environ.* **2020**, *716*, 137095. [[CrossRef](#)]
18. Zhu, H.; Zhang, D.; Wang, T.; Wu, H.; Li, V.C. Mechanical and self-healing behavior of low carbon engineered cementitious composites reinforced with PP-fibers. *Constr. Build. Mater.* **2020**, *259*, 119805. [[CrossRef](#)]
19. Şahmaran, M.; Li, V.C. Durability properties of micro-cracked ECC containing high volumes fly ash. *Cem. Concr. Res.* **2009**, *39*, 1033–1043. [[CrossRef](#)]
20. Kuroda, M.; Watanabe, T.; Terashi, N. Increase of bond strength at interfacial transition zone by the use of fly ash. *Cem. Concr. Res.* **2000**, *30*, 253–258. [[CrossRef](#)]
21. Sun, R.; Hu, X.; Ling, Y.; Zuo, Z.; Zhuang, P.; Wang, F. Chloride diffusion behavior of engineered cementitious composite under dry-wet cycles. *Constr. Build. Mater.* **2020**, *260*, 119943. [[CrossRef](#)]
22. British Standard Institution. *BS EN 197-1:2011, Cement, Composition, Specifications, Conformity Criteria for Common Cements*; British Standard Institution: London, UK, 2011.
23. ASTM. *Standard Test Method for Electrical Indication of Concrete's Ability to Resist Chloride Ion Penetration*; ASTM C1202; ASTM: West Conshohocken, PA, USA, 2019.
24. Dean, S.; Bassuoni, M.; Nehdi, M.; Greenough, T. Enhancing the Reliability of Evaluating Chloride Ingress in Concrete Using the ASTM C 1202 Rapid Chloride Penetrability Test. *J. ASTM Int.* **2006**, *3*, 1–13. [[CrossRef](#)]
25. Edvardsen, C.; Jepsen, M.T.; Andrade, C.; Kropp, J. Chloride migration coefficients from non-steady-state migration experiments at environment-friendly “Green” concrete. In Proceedings of the Second International RILEM Workshop on Testing and Modelling the Chloride Ingress into Concrete, Paris, France, 11–12 September 2000; pp. 203–209.
26. Chindaprasirt, P.; Jaturapitakkul, C.; Sinsiri, T. Effect of fly ash fineness on microstructure of blended cement paste. *Constr. Build. Mater.* **2007**, *21*, 1534–1541. [[CrossRef](#)]
27. Maso, J. The bond between aggregates and hydrated cement pastes. In Proceedings of the 7th International Congress on the Chemistry of Cement, Paris, France, 1 January 1980; pp. VII-1/3–VII-1/15.
28. Thomas, M.D.; Bamforth, P.B. Modelling chloride diffusion in concrete: Effect of fly ash and slag. *Cem. Concr. Res.* **1999**, *29*, 487–495. [[CrossRef](#)]
29. Leng, F.; Feng, N.; Lu, X. An experimental study on the properties of resistance to diffusion of chloride ions of fly ash and blast furnace slag concrete. *Cem. Concr. Res.* **2000**, *30*, 989–992. [[CrossRef](#)]
30. Glass, G.; Reddy, B.; Buenfeld, N. The participation of bound chloride in passive film breakdown on steel in concrete. *Corros. Sci.* **2000**, *42*, 2013–2021. [[CrossRef](#)]
31. Glass, G.; Reddy, B.; Buenfeld, N. Corrosion inhibition in concrete arising from its acid neutralisation capacity. *Corros. Sci.* **2000**, *42*, 1587–1598. [[CrossRef](#)]
32. Ahmad, S. Reinforcement corrosion in concrete structures, its monitoring and service life prediction—A review. *Cem. Concr. Compos.* **2003**, *25*, 459–471. [[CrossRef](#)]
33. Pacheco, J.; Polder, R. Corrosion initiation and propagation in cracked concrete—a literature review. In *Advances in Modeling Concrete Service Life*; Springer: Berlin/Heidelberg, Germany, 2012; pp. 85–93.
34. Chatterji, S. On the applicability of Fick’s second law to chloride ion migration through Portland cement concrete. *Cem. Concr. Res.* **1995**, *25*, 299–303. [[CrossRef](#)]

35. Liu, T.; Weyers, R. Modeling the Dynamic Corrosion Process in Chloride Contaminated Concrete Structures. *Cem. Concr. Res.* **1998**, *28*, 365–379. [[CrossRef](#)]
36. Zhang, J.; Wang, J.; Kong, D. Chloride diffusivity analysis of existing concrete based on Fick's second law. *J. Wuhan Univ. Technol. Sci. Ed.* **2010**, *25*, 142–146. [[CrossRef](#)]
37. Torres-Luque, M.; Bastidas-Arteaga, E.; Schoefs, F.; Sánchez-Silva, M.; Osma, J. Non-destructive methods for measuring chloride ingress into concrete: State-of-the-art and future challenges. *Constr. Build. Mater.* **2014**, *68*, 68–81. [[CrossRef](#)]
38. Koteš, P.; Strieška, M.; Bahleda, F.; Bujňáková, P. Prediction of RC Bridge Member Resistance Decreasing in Time under Various Conditions in Slovakia. *Materials* **2020**, *13*, 1125. [[CrossRef](#)]